

Experimental Stress Analysis of the TF-30 Turbine Engine Third-Stage Fan-Blade/Disk Dovetail Region

V. J. PARKS and R. J. SANFORD

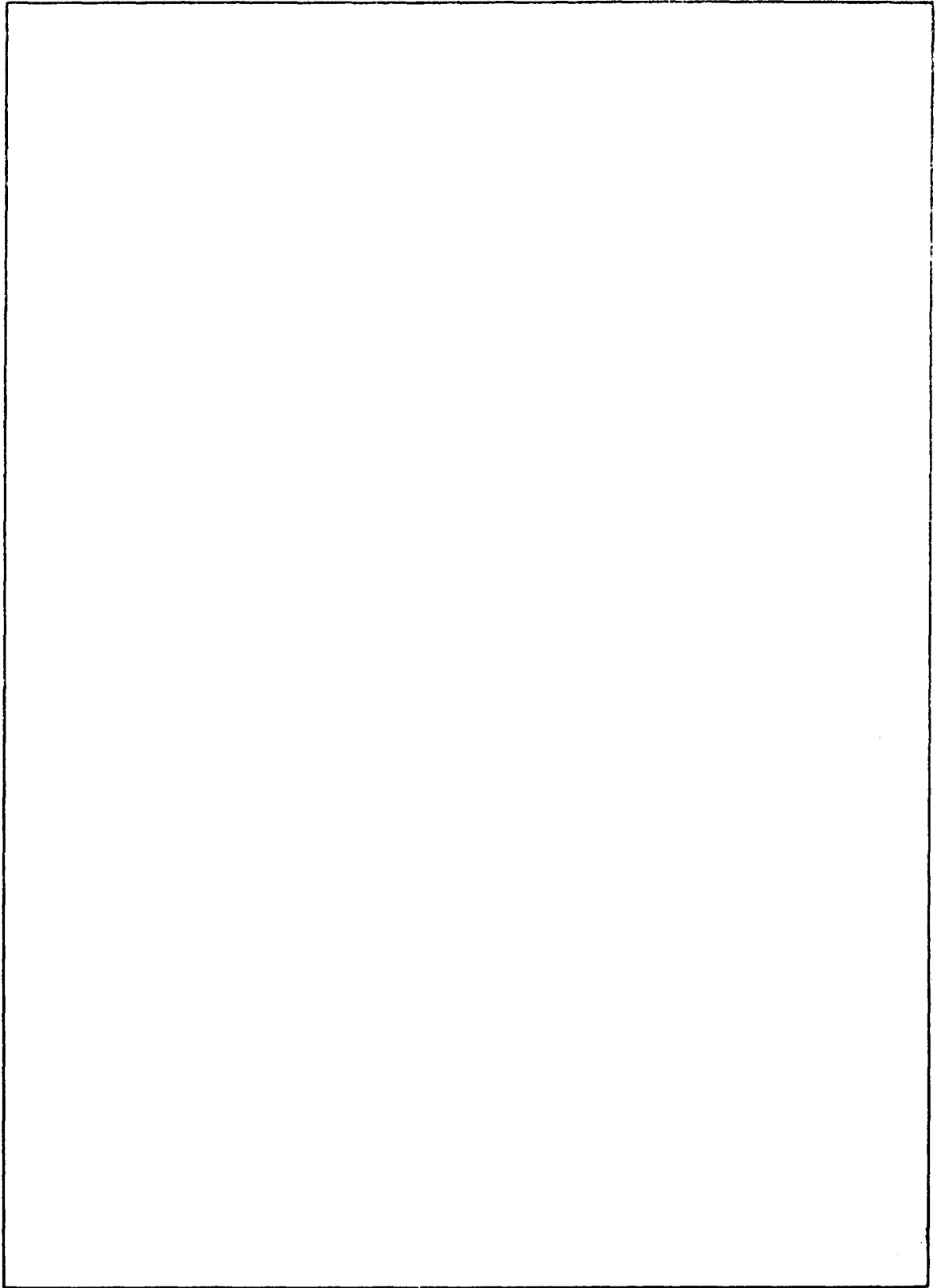
Ocean Technology Division

August 26, 1977



NAVAL RESEARCH LABORATORY
Washington, D.C.

Approved for public release; distribution unlimited.



CONTENTS

INTRODUCTION	1
METHODS OF ANALYSIS	1
EXPERIMENTAL PROCEDURES	3
STRESS CONCENTRATION FACTORS	8
STRESS DISTRIBUTIONS	15
DIRECTION, MAGNITUDE, AND POSITION OF BEARING SURFACE LOADS	16
FILLET MODIFICATIONS TO REDUCE FILLET STRESS ...	20
STRESSES ON THE BEARING SURFACE ADJACENT TO THE FILLET	24
SUMMARY	24
APPENDIX A — Stress Concentration Factors by Heywood's Method	26
REFERENCES	29

EXPERIMENTAL STRESS ANALYSIS OF THE TF-30 TURBINE ENGINE THIRD-STAGE FAN-BLADE/DISK DOVETAIL REGION

INTRODUCTION

Several in-service failures of the TF-30 turbojet engine used in the F-14 aircraft have been traced to cracking in the third-stage fan-blade/disk assembly, shown in Fig. 1. The overall diameter of this assembly is 32.5 in. (0.83 m). A close-up view of the blade/disk dovetail region is shown in Fig. 2. In this study attention is limited to this region. Figure 3 shows four disk lugs with fatigue cracks, indicated with dye-penetrant. The disk which was removed from service had similar cracks in 15 out of the total of 36 lugs. Low-power microscopic examination (30X) of the cracks indicates that most of the 14 cracks on the right side of the lugs appear to originate under the bearing surface, whereas the two cracks on the left side of the lugs appear to originate inboard of the bearing area, i.e., at the beginning of the fillet region.

It was initially believed that the cause of these failures was a loss of airseal constraint on the third-stage blades due to accelerated wear. This condition would result in an increase in vibratory stress on the third-stage disk; such stress could result in ultimate fatigue failure. However, after rework of the engines to solve this problem, third-stage disk failures continued. Periodic examination of the reworked engines indicated that there were cracks in numerous disk lugs after as little as 80 hours of service operation. The design of the third-stage fan assembly of the TF-30 engine was based upon the results of a thorough analysis of a similar engine, the JT-8D; however, no such analysis has been performed on the TF-30 third stage.

Primary consideration in this report is given to the loads produced by centrifugal forces as the disk and its 36 blades are rotated. The centrifugal force exerted by each blade must be carried by the blade surfaces which are in contact with the mating surfaces on the disk. These surfaces are subsequently termed either load-bearing surfaces or simply bearing surfaces.

Other in-service loads acting on the disk-blade assembly that might contribute to cracking, but were considered less important, are the gas loads on the blades, centrifugal forces on the disk both above and below the bearing surface, thermal gradients, and low-level vibratory stresses on the disk.

METHODS OF ANALYSIS

Various theoretical and experimental methods are available to evaluate the stresses in the fillet regions of the disk and blades. The approximately uniform cross section of the disk lugs and the blade below the platform suggested a two-dimensional analysis of

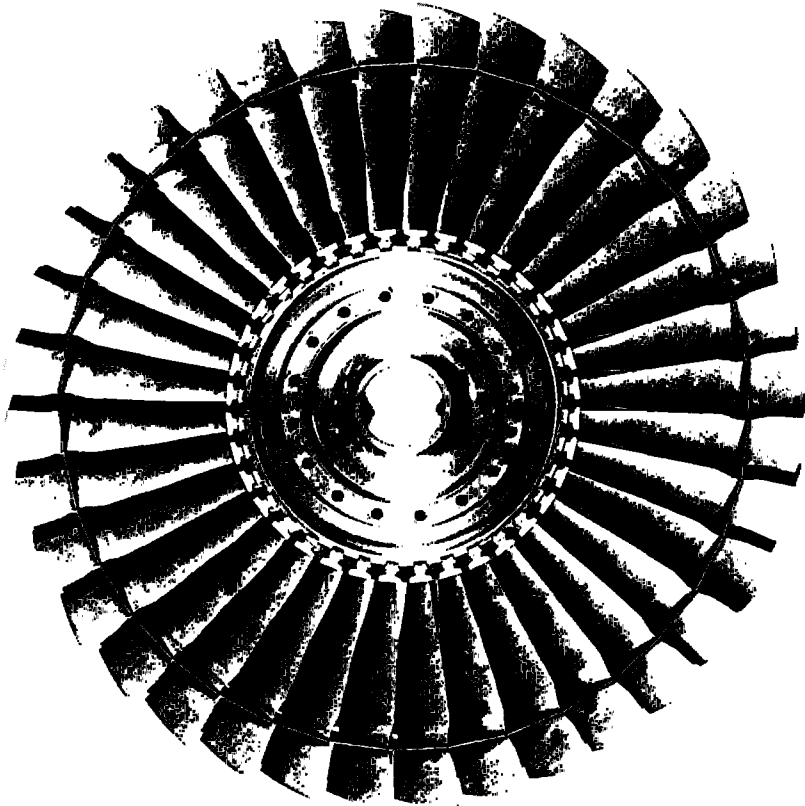


Fig. 1 — Assembled TF-30 third-stage disk with 36 blades (overall diameter, 32.5 in. (0.83 m))

the region of interest. Both numerical and experimental approaches were used. A complementary 2-D finite element analysis has been conducted and will be reported separately. The finite element method permits a variation of load parameters not possible with the experimental method. A formula to obtain "tooth" stresses was also applied, and the results are reported in the Appendix. These theoretical solutions require specifying the magnitude, position, and direction of the tooth loads in one form or another. The experimental study was conducted to simulate the loads on the bearing surface more directly without specifying a priori the loading conditions in the contact region. Two experimental approaches were used: photoelasticity and photoelastic holography. Isochromatic and isoclinic patterns were obtained using a sodium diffused-light polariscope of conventional design. Isopachic patterns were obtained using a recently developed holographic polariscope [1] which facilitates absolute retardation measurements. The holographic polariscope gives sufficient data for a complete stress analysis [2]; however, it was found more efficient to use both methods.

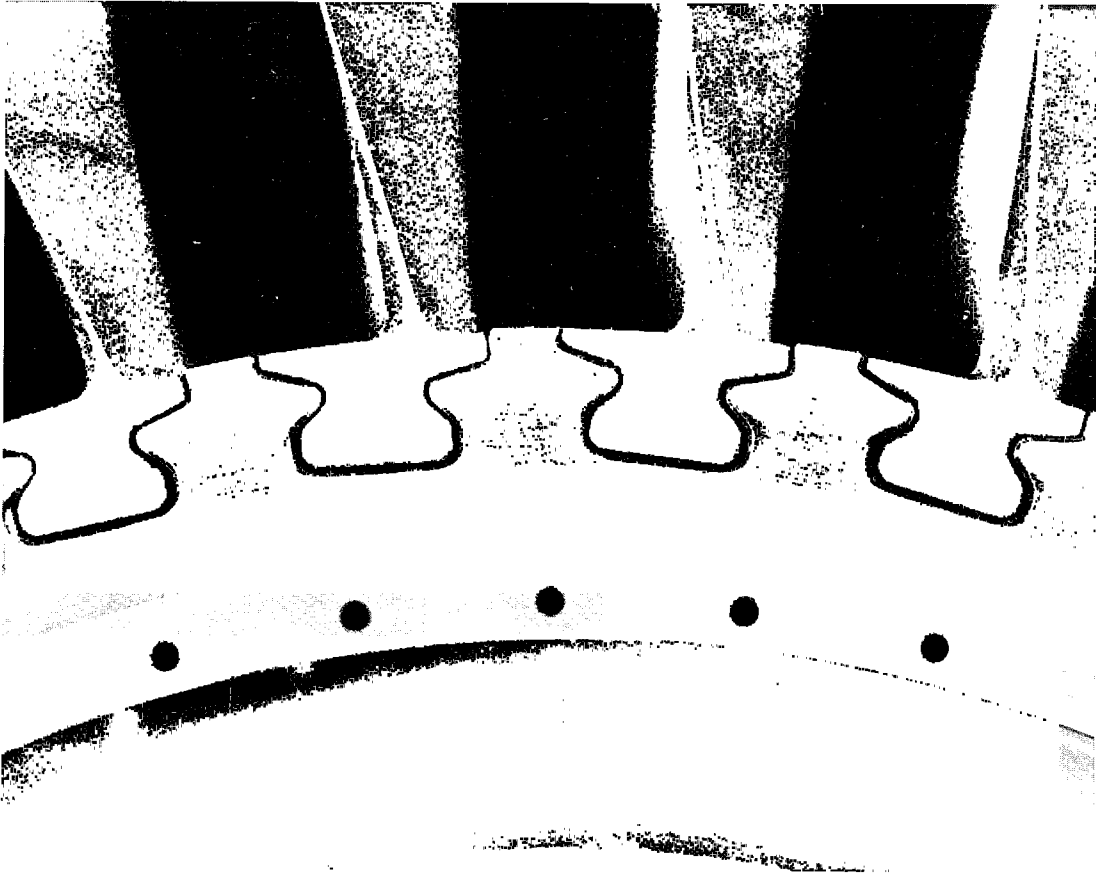


Fig. 2 — TF-30 third-stage blade/disk dovetail region

Each method provided information used in determining the complete stress field. Isoclinics give the directions of the principal stresses throughout the field. The isochromatics, with calibration, give the difference of principal stresses through the field and the tangential stresses on all free edges. The isopachics, with calibration, give the sum of the principal stresses throughout the field. Half of the sum of the isochromatics and isopachics gives one principal stress, and half of the difference gives the other. Thus, the complete stress field in two dimensions, i.e., both principal stresses and their direction, can be determined at any point from the isochromatics, isopachics, and isoclinics.

EXPERIMENTAL PROCEDURES

To represent the disk/blade dovetail region, two disk slots were modeled. Figure 4 shows the disk model; it represents the disk lug in the region between the slots. Figure 5 shows the blade model geometry. The blade models simulate the blade cross section in the area below the platform. The region above the platform was made uniform for a sufficient length, and then a reduced width shank region was added for calibration purposes. An area for clamping was left at the far end of the blade model.

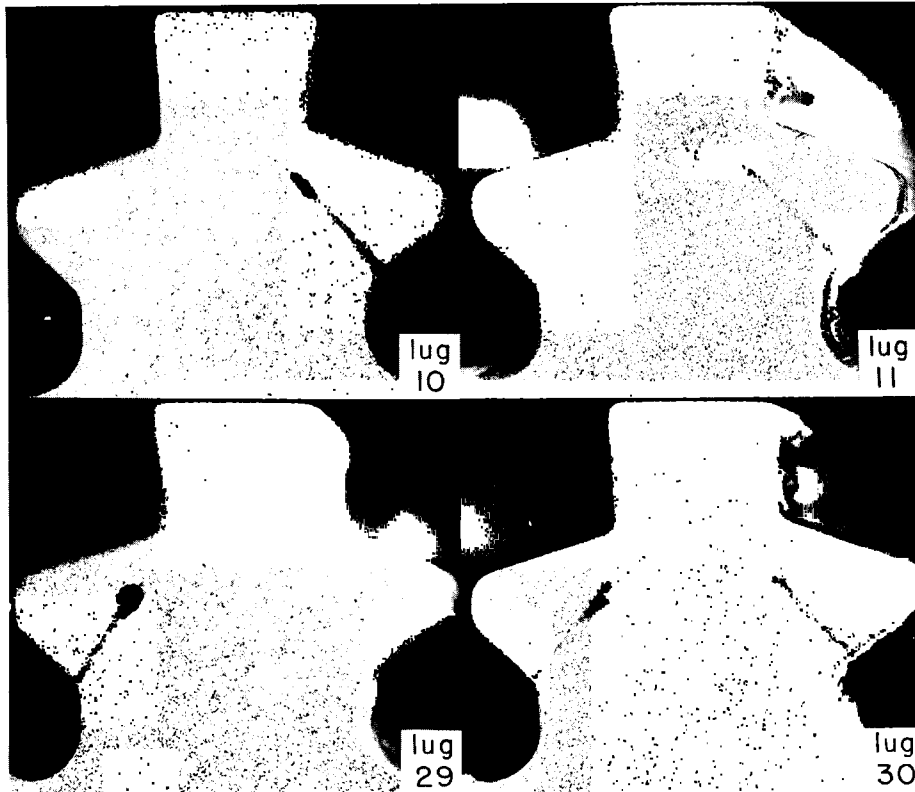


Fig. 3 — Dye penetrant indications of typical fatigue cracks in a disk removed from service

Model dimensions are shown in Figs. 4 and 5; these dimensions are 3.409 times the actual dimensions. To simplify the loading, the disk model was dimensioned so that the loads acting along the blade axes were parallel to each other. This simplification eliminates the 5° angle between blade and disk lug axes but does not introduce significant error into the analysis. The parallel distance between the blade axes for the model was scaled from the circumferential distance between the blade axes at the centerline of the bearing area.

The dimensions shown in Figs. 4 and 5 were first cut with a Gordon numerical controlled milling machine on aluminum plate 1/8 in. (3.2 mm) thick. The dimensions shown were cut in steps of 0.001 in. (0.025 mm). To insure a smooth bearing surface on the template and model, the computer program was written so that the edges of the bearing surfaces coincided with the orthogonal cutting directions of the milling machine. The 3.409 scale was chosen so that the 0.055 in. (1.40 mm) fillet would be cut in a continuous cut by a 3/8 in. (9.5 mm) milling cutter.

The aluminum templates were fixed with double-backed adhesive tape to a plastic sheet 1/4 in. (6.4 mm) thick. The plastic sheet was saw cut to within 1/16 in. (1.6 mm) of the template edge. The plastic was then machined to the template shape with a high-speed two-flute tungsten-carbide cutter rotating at 45,000 rpm, guided by a pin of equal diameter that followed the template edge.

PARKS AND SANFORD

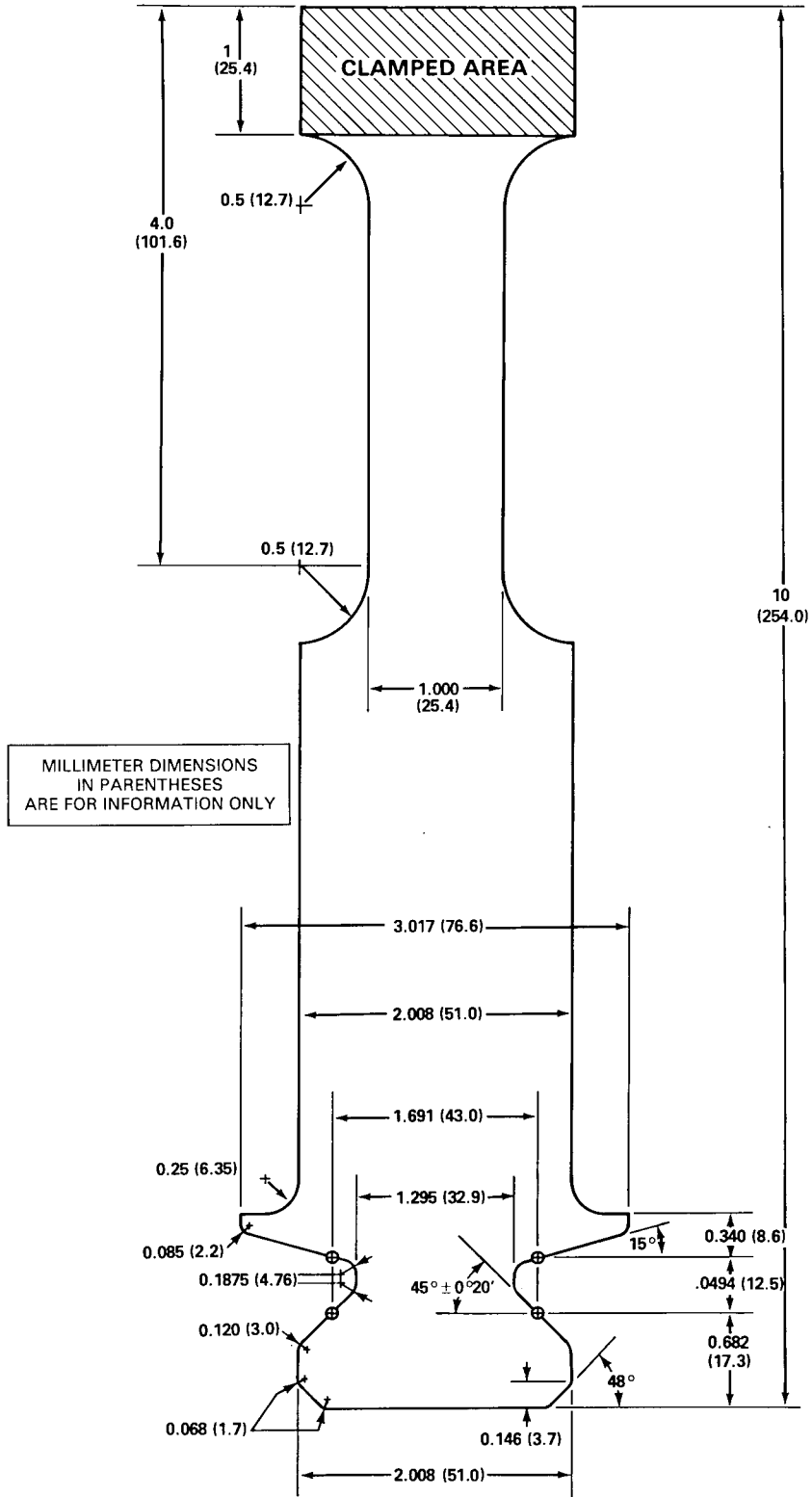


Fig. 5 — Blade model

Models were made out of both Homalite 100* and Plexiglas II (UVA).† The models were approximately 1/4 in. (6 mm) thick. The Homalite 100 models were analyzed in the standard polariscope for isochromatics and isoclinics. The Plexiglas II models were analyzed for isopachics in the holographic polariscope and for isoclinics in the standard polariscope. It would have been possible to perform the complete analysis with just the Homalite 100 models; however, the Plexiglas II models served two useful purposes, which simplified the analysis procedure. Plexiglas II is insensitive to the photoelastic effect, i.e., the stress difference (isochromatic) photoelastic constant is nearly (but not exactly) zero; accordingly, the isoclinic lines clearly stand out in the photographs taken with the standard polariscope. Similarly, while the isochromatic response of Plexiglas II is small, the isopachic photoelastic response, which is important in the holographic analysis, is large. Therefore, the double-exposure holographic patterns from the Plexiglas II models contain only isopachic fringes, and potential problems in interpretation of the fringe patterns are avoided [3].

To load the models, steel clamps were mounted to the ends of the two blade models, and a steel frame was mounted on three sides of the disk model, as indicated in Figs. 4 and 5. The clamps were on both sides of the models and were held together and to the models with screws not shown in the figures. Clearance holes were drilled through the models for the screws. Abrasive paper was cemented to the steel clamps to prevent slippage and to transmit the load to the models. The complete model, including the frame and clamps, was mounted in a small universal testing machine equipped to apply an equal and uniform tension to both blade models while the frame of the disk model was held rigid. This as a first approximation represents the centrifugal load on the engine blades and on the disk. The bearing surfaces between the blades and lugs were lubricated with a molybdenum disulfide high-pressure lubricant‡ to simulate the prototype conditions.

Isochromatic patterns were photographed for all of the Homalite models at loads of 320 lb (1420 N) and 640 lb (2850 N). Isopachics were taken from the Plexiglas models at net loads of 500 lb (2220 N) and 250 lb (1110 N). Isoclinics were taken from the Plexiglas model at a 500-lb (2220-N) load in the standard polariscope with white light. Various other patterns at various loads were obtained. Calibration beams of both Plexiglas II and Homalite 100 were loaded to measure the stress-optic constants of the materials and to check the self-calibration of the blade shank. Various data obtained are summarized in Tables 1 and 2.

Representative photographs of various fringe patterns are shown in Figs. 6 through 9. Figure 6 shows the dark field isochromatic pattern of the whole model at 640 lb (2850 N). An enlarged photograph of the same pattern showing the details of the fringes for just the lug region is shown in Fig. 7. An isopachic pattern showing one full blade and lug for the Plexiglas II model taken in the holographic polariscope is shown in Fig. 8. Unlike the photoelastic patterns where white light was used as an aid in determining the order (number) associated with each fringe, the holographic method by its nature requires monochromatic light; alternate methods are needed to identify fringe order. One such method is the use of ramp loading while recording the hologram [4]. In this method the

*Homalite Corporation, Wilmington, Del.

†Rohm and Haas, Philadelphia, Pa.

‡Moly-lube Anti-Seize, Bel-Ray Co., Farmington, N. J.

PARKS AND SANFORD

Table 1 — Summary of Photoelastic Tests (Sodium Light Polariscopes, 5893Å)

Case No.	Model		Load		Type of Pattern
	Geometry	Mat'l	(lb)	(N)	
1	Original	H-100*	320	1420	Light and dark field isochromatics, overall model
		H-100	640	2850	Light and dark field isochromatics, overall model
		H-100	640	2850	Light and dark field isochromatics, lug only
		H-100	640	2850	Light and dark field isochromatics, blade only
2	Original	P-II**	500	2220	Isoclinics, 0°, 5°, 10°, 20°, 30°, 40°, 50°, 60°, 70°, 80°, 85°
3	Hand filed #1	H-100	630	2800	Light and dark field isochromatics, overall model
		H-100	630	2800	Light and dark field isochromatics, lug only
4	Hand filed #2	H-100	640	2850	Same sequence as Case 3
		H-100	640	2850	
5	Final modified geometry	H-100	320	1420	Same sequence as Case 1
		H-100	640	2850	
		H-100	640	2850	
		H-100	640	2850	

*Homalite 100 **Plexiglas II

zeroth order fringe appears as a bright (white) fringe with higher order fringes progressively less distinct. A typical pattern is shown in Fig. 9.

A composite sketch of the isoclinics in the blade model made from the eleven separate isoclinic photographs taken at eleven different settings of the polariscopes as listed in Table 1 is shown in Fig. 10. This isoclinic map was used to determine the coefficient of friction of the model. Full details of the procedure are given in Section titled Direction, Magnitude, and Position of Bearing Surface Loads.

STRESS CONCENTRATION FACTORS

The isochromatic patterns provide the stress concentration factors in the fillets of both the disk lug and the blades. The choice of a definition for the concentration factor (s.c.f.) is somewhat arbitrary and will be defined here as the ratio of the maximum tensile stress along the fillet edge to the average stress in the minimum section of the disk lug. Since the area of the minimum section is known, this average stress can always be calculated if the load is known.

Table 2 — Summary of Tests Conducted With Holographic Polariscope (5145Å)

Case No.	Model		Loads (see note)		Type of Pattern
	Geometry	Mat'l	(lb)	(N)	
1	Original	H-100*	550 & 50	2450 & 220	Vertical and horizontal polarization
		H-100	300 & 50	1330 & 220	Vertical and horizontal polarization
		H-100	300 & 100	1330 & 440	Circular polarization
		H-100	300	1330	Light field isochromatics (single exposure)
2	Beam in bending	H-100	600 & 200	2670 & 890	Circular polarization
		H-100	150 in.-lb	16.9 N-m	Light field isochromatics (single exposure)
		H-100	170 & 20 in.-lb	19.2 & 2.3 N-m	Vertical polarization
		H-100	100 & 50 in.-lb	11.3 & 5.6 N-m	Vertical and horizontal polarization
3	Original	P-II**	300 & 50	1330 & 220	Vertical, horizontal, and circular polarization
		P-II	550 & 50	2450 & 220	Circular polarization
		P-II	500 to 100	2220 to 440	Circular polarization (single exposure—ramp load)
4	Beam in bending	P-II	200 & 50 in.-lb	22.6 & 5.6 N-m	Vertical, horizontal, and circular polarization
		P-II	200 in.-lb	22.6 N-m	Dark field & light field isochromatics (single exposure)
5	Beam in bending	H-100	170 & 20 in.-lb	19.2 & 2.3 N-m	Horizontal polarization

*Homalite 100

Note: All holograms were double-exposure type except as noted.

**Plexiglas II

The stress-optic law for uniaxial stress such as on an unloaded boundary is

$$\sigma = \frac{nf}{t} , \tag{1}$$

where

σ is the stress at a point in the shank or on the free edge

n is the fringe order at the same point

t is thickness of the model

f is the material fringe value (the photoelastic constant).



Fig. 6 — Dark field isochromatic pattern of model of blade/disk dovetail region

The corresponding s.c.f. is

$$\frac{\sigma}{\sigma_{av}} = \frac{nf/t}{P'/A} \quad (2)$$

where

σ_{av} is the average stress in the disk neck

A is the minimum disk lug area ($A = tw$)

P' is the total vertical load on the disk lug (also on the blade)

w is the width of the minimum section of the lug.

The s.c.f. could be determined from this formula; however, in this analysis an auto-calibration approach was used. The stress in the shank of the blade model also satisfies Eq. (1); so

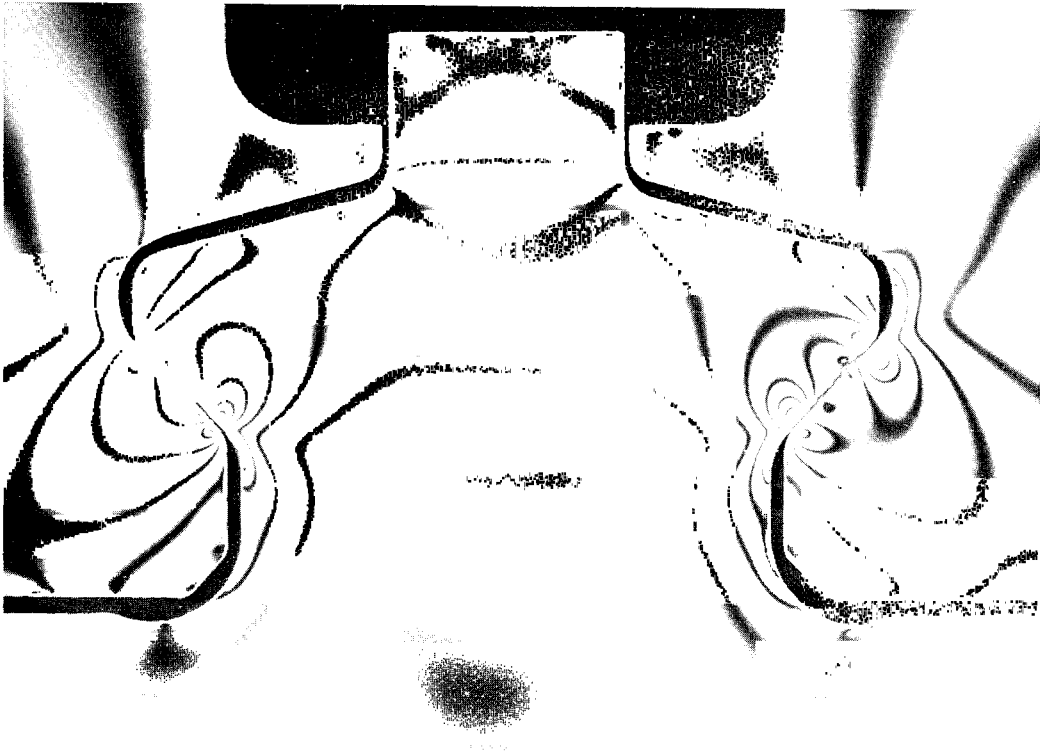


Fig. 7 — Dark field isochromatic pattern of model of disk lug

$$\sigma_s = \frac{P'}{A_s} = \frac{n_s f}{t_s}, \quad (3)$$

where

σ_s is the uniaxial stress in the shank

A_s is the shank area ($A_s = t_s w_s$)

n_s is the shank fringe order

t_s is the shank thickness

w_s is the shank width.

From Eq. (3) the fringe value f can then be written

$$f = \frac{P'}{n_s w_s}. \quad (4)$$

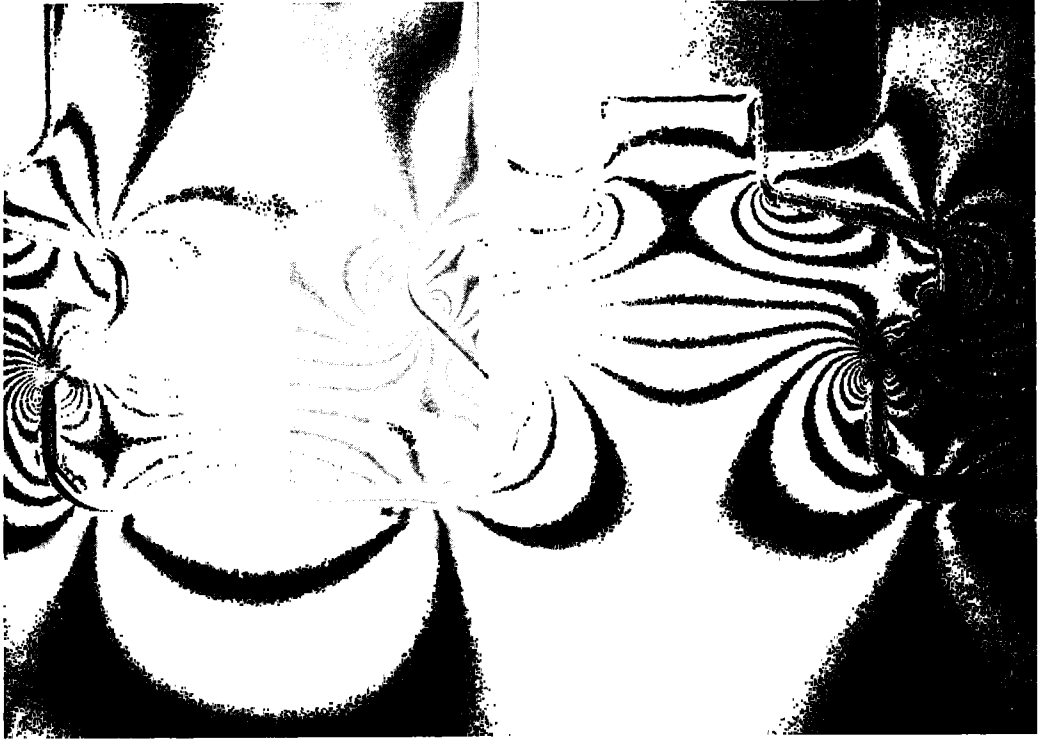


Fig. 8 — Holographic pattern of isopachics of model of blade/disk dovetail region

By substituting Eq. (4) into Eq. (2), one can express the s.c.f. as

$$\frac{\sigma}{\sigma_{av}} = \frac{n}{n_s} \frac{w}{w_s}$$

The s.c.f. in the fillet is equal to the ratio of the fringes in the fillet to the fringe in the calibration shank, modified by the ratio of the width in the net section of the lug to the width in the shank. This autocalibration approach eliminates the need to use, or even determine, the load P' and the fringe value f .

In determining the s.c.f.'s, every attempt was made to keep the blade loads equal and the individual tooth loads equal and symmetric. It was possible to obtain symmetric patterns over most of the model, but in the regions of the bearing surfaces, this was impossible. Each contact region possessed an individual pattern associated with how the contact was made. The individual fillet fringes varied slightly with the variation of magnitude, position, and direction of the contact loads. In determining s.c.f.'s, the average of the fringes in all four fillets was used. The implications of this are discussed in detail in a later section.

The s.c.f.'s as described above were:

for the fillet of the disk = 5.2
for the fillet of the blade = 4.8



Fig. 9 — Reconstructed time average hologram to locate the zero values of the isopachics

Both of these values are in terms of the average stress in the disk lug. If the s.c.f. for the blade is desired in terms of the average stress in the net section area of the blade, it is only necessary to multiply by the ratio of the respective widths ($1.295/1.722 = 0.752$).

The s.c.f. in the fillet of the blade in terms of the average stress in the blade net section is 3.6.

To illustrate the s.c.f. in terms of stresses, consider a blade revolving at 10,500 rpm that weighs 0.738 lb (3.28 N) and has a centroid at $r_0 = 10.75$ in. (273 mm) from the axis of the disk. The force due to the weight of the blade will be

$$F = \frac{\text{weight}}{g} \omega^2 r_0,$$

where g is the acceleration of gravity, 386 in/sec^2 (9.80 m/sec^2) and ω is the speed of rotation in radians/sec. Therefore,

$$F = \frac{0.738}{386} \left[10,500 \frac{2\pi}{60} \right]^2 (10.75) = 24,900 \text{ lb (110.7 kN)}.$$

This is the force that would act on the bearing surface. An analysis was made of the blade geometry, and it was found that the force passing through the neck of the blade would be about 96% of this load. Assuming the disk lug to be about the same weight as the blade lug, the total load on the neck of the disk lug would be about 104%

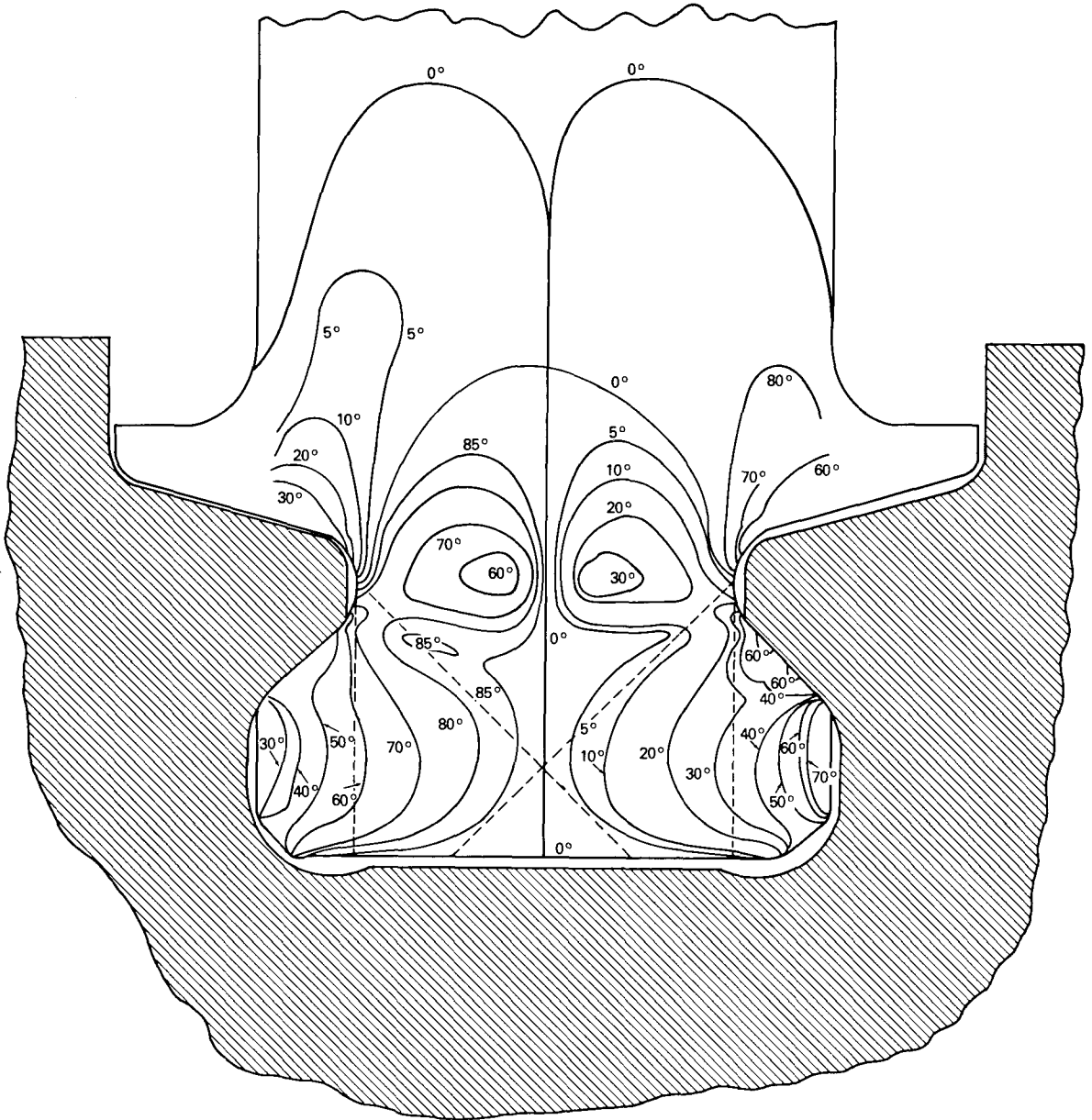


Fig. 10 — Complete isoclinic pattern of one of the blades

of this load. In the following illustration the 24,900 lb (110.7 kN) load will be used. The net section of the disk just below the fillet has an area of 1.138 in.² (734 mm²). The average stress in the net section is then 24,900/1.138 = 21,900 psi (151 MPa).

The estimated maximum stress in the fillet of the disk is

$$\sigma_D = (21,200) (5.2) = 114,000 \text{ psi (786 MPa)}$$

and in the blade is

$$\sigma_B = (21,200) (4.8) = 105,000 \text{ psi (724 MPa)}.$$

Note that any variation in the engine speed will vary the stresses by the square of the speed change. Thus, if the speed is increased 10% the stress will increase by 21% = 100(1.1² - 1).

STRESS DISTRIBUTIONS

Stresses along the entire free boundary of the fillet can be obtained just as the s.c.f.'s were obtained. The tangential stress distributions along the fillets of the disk and blade are given in Figs. 11 and 12.

Stresses away from the free boundaries were determined by combining the isochromatic and isopachic data. The isochromatics were normalized by autocalibration as in the s.c.f. analysis. In the holographic polariscope it was not convenient to record isopachic fringe orders on the shank of the blade for autocalibration. A beam of the Plexiglas material was loaded with a pure moment, and the isopachic fringe orders were recorded on a hologram in the holographic polariscope. This pattern gave an isopachic fringe value of 33.7 psi-in/fringe (5.90 kPa-m/FR).

The isopachic fringe orders were multiplied by the isopachic fringe value and divided by the average stress in the disk net section. These calculations gave normalized isopachics similar to the normalized stresses represented by Eq. 2. The normalized isopachics $(\sigma_1 + \sigma_2)/\sigma_{av}$, the normalized isochromatics $(\sigma_1 - \sigma_2)/\sigma_{av}$, half their sum σ_1/σ_{av} , and half their difference σ_2/σ_{av} are shown for a horizontal line through the point of maximum stress on the fillet of the disk in Fig. 13. The corresponding set of curves for the neck of the blade is given in Fig. 14. A third set of the curves was obtained (Fig. 15) for a line through the point of maximum stress in the fillet of the disk and tangential to the fillet boundary. Typical cracks have been observed along this line (see Fig. 3).

These stress distributions indicate a rather sharp dropoff of the maximum principal stress in directions normal to the fillet boundaries, as opposed to the gradual dropoff of the fillet stress along the free boundary as shown in Figs. 11 and 12. This is typical of fillet stress distributions.

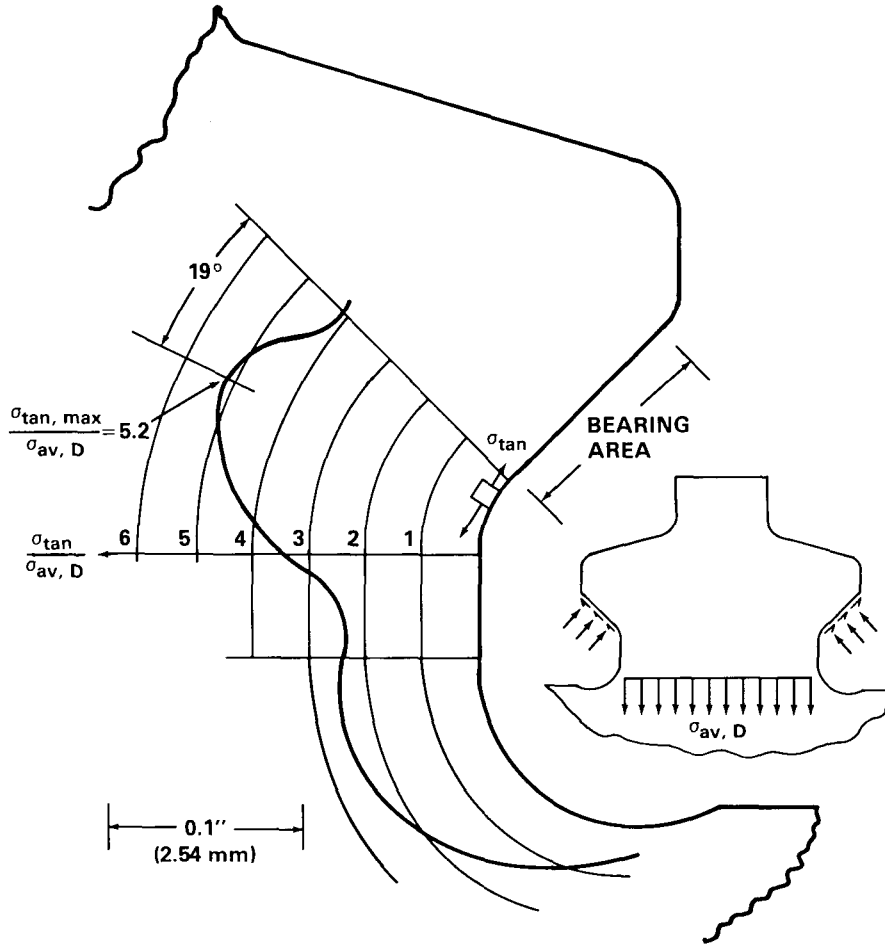


Fig. 11 — Tangential boundary stress in fillet of disk

DIRECTION, MAGNITUDE, AND POSITION OF BEARING SURFACE LOADS

As noted above, unlike the requirements for theoretical analysis, it is not necessary in the model to specify the direction, magnitude, or position of load on the bearing surfaces. The loads are applied remotely, two equal loads applied along the blade axes. From the experimental analysis the direction and magnitude of load on both bearing surfaces can be determined. This is most simply done by calculating the shear stresses along two lines which pass through the blade and isolate the load-bearing area from the rest of the blade. These lines are shown as dotted lines in the isoclinic pattern (Fig. 10). A free-body diagram of the area isolated by the line will show two forces acting parallel to the line: (1) the force due to shear stress along the line and (2) the component of the bearing-surface force parallel to the line. Equating these two forces allows solution of the component of the bearing-surface force.

It was found convenient to use two lines, one normal to the load-bearing surface, and one vertical. The line normal to the load-bearing surface (the long diagonal) gives

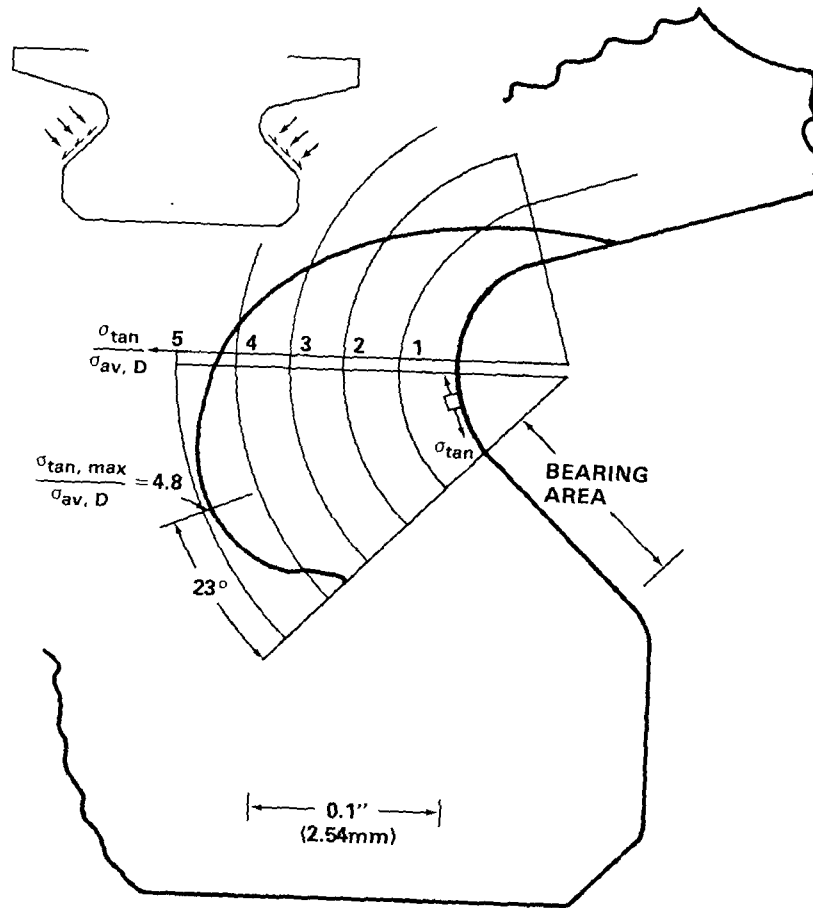


Fig. 12 — Tangential Boundary stress in fillet of blade

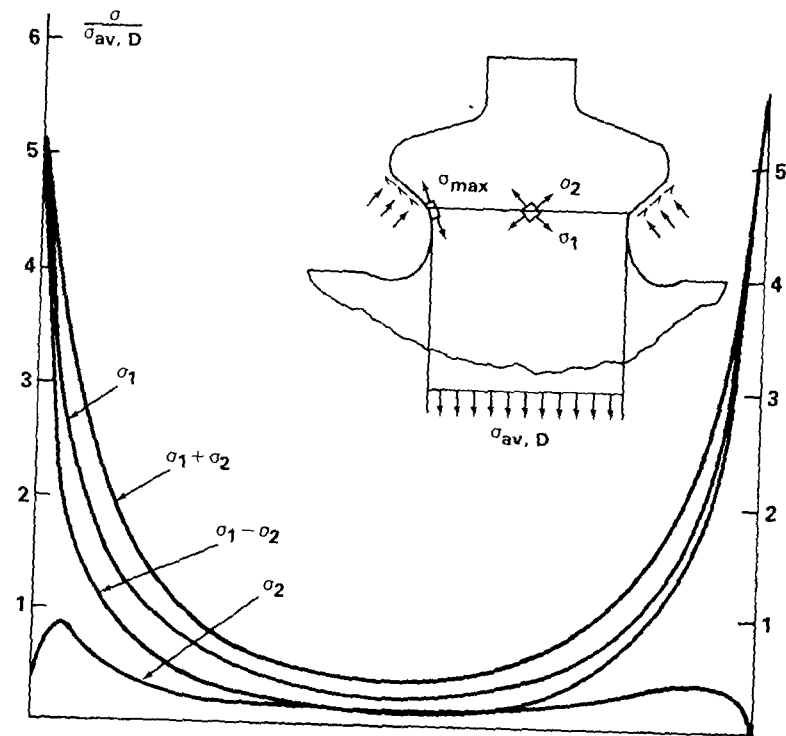


Fig. 13 — Principal stresses along a horizontal line across the neck of the disk. The line ends at the points in the fillet which are subjected to the maximum stress.

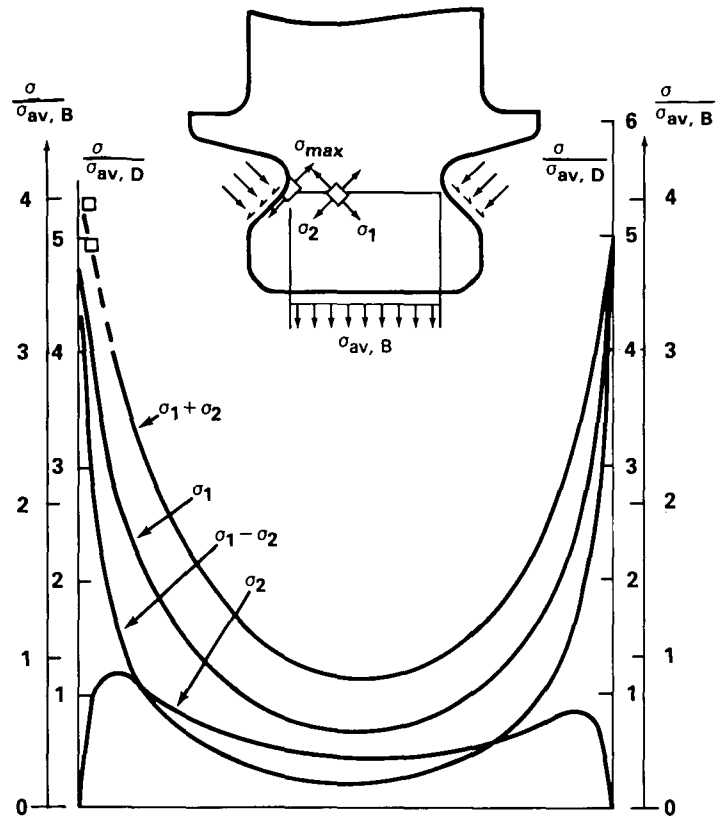


Fig. 14 — Principal stress along a horizontal line across the neck of the blade. The line ends at the points in the fillet which are subjected to the maximum stress.

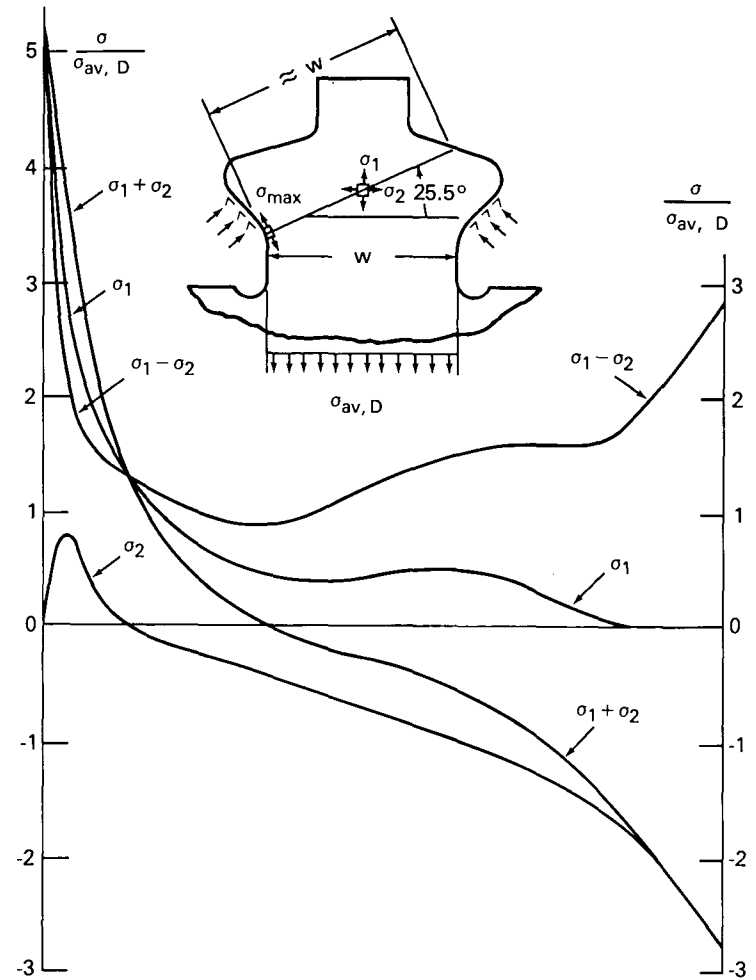


Fig. 15 — Principal stresses along the line through the point of maximum tensile stress in the disk fillet. The line is perpendicular to the boundary at the point (average of left and right sides).

the normal component of load on the bearing surface directly; the vertical line gives the vertical component. A simple vector analysis gives the tangential component of load (the friction force). The ratio of tangential to normal load can be used as an estimate of the average coefficient of friction along the bearing surface.

Shear stress on any plane is given by

$$\tau_{xy} = 1/2(\sigma_1 - \sigma_2) \sin 2\Theta,$$

where

- τ_{xy} is the shear stress at any point in the x and y direction
- σ_1 and σ_2 are the principal stresses at the point
- Θ is the angle between the x - y directions and the principal directions.

Isochromatics give $(\sigma_1 - \sigma_2)$; Isoclinics give Θ . Therefore, shear stresses in any direction along any line can be determined from the isochromatics and the isoclinic map of Fig. 9.

The area under each curve of shear-stress vs position was measured, calibrated, and multiplied by the thickness to determine the corresponding forces. The forces obtained by this method for both sides of the blade, in terms of the load applied to the blade are given in Table 3.

Note that without friction because of the 45° angle of the bearing surface the normal components of load would be 70.7% of the total axial load. The variation of friction between the left and right sides is probably due to the tendency of the friction surfaces to slip in steps, so that the tangential load may vary 2% or 3% as the load changes.

Determining the position of the load is more involved than determining direction and magnitude. The actual disk and blade are designed to make contact in the unloaded state not at one point or position, but over the entire bearing surface. Under load, long contact regions tend to have higher loads in the central region. In addition, if the blade and disk bearing surfaces have different amounts of angular deformation (i.e., compliance) under load, the mating surfaces will tend to open up at the end which has the greater angular deformation. The blade appears to be stiffer than the disk, indicating a shift of the load towards the base of the disk, and towards the tip of the blade. If such a difference does occur under load, it is likely to occur primarily on one side of each blade, leaving the other side in more uniform contact.

Table 3 — Loads on Bearing Surfaces in Terms of Radial Load on Blade

Parameter	Left Side	Right Side
Radial component of load	49.0%	51.0%
Tangential component of load	7.8%	10.1%
Friction factor	0.126	0.164

This effect is illustrated in the fringe pattern shown in Fig. 6. In this example the contact is more uniform on the right side of each blade, leaving the left side in essentially point contact near the base of the bearing area. It is felt that this nonsymmetry due to variation in contact is more severe in the engine than in the model since the engine material is more rigid, the dimensions of the engine are smaller, and the manufacturing of the engine parts is probably no more exact than that of the model.

Nevertheless, for the analysis to be meaningful it is necessary, insofar as possible, to maintain symmetry. As in a theoretical analysis, the symmetry is an idealization, which is necessary to make the model representative of the average or "idealized" engine disk lug and blade.

This all means that the positions and distributions of load shown in Figs. 6, 7 and 8 are "representative" of the actual loads.

FILLET MODIFICATIONS TO REDUCE FILLET STRESS

Although the original intent of this program was solely to determine the stress in the existing blade/disk dovetail region, it was found that, with little additional effort, it was possible to do some preliminary redesign analysis of the disk fillet region. As a first step the original models and templates were used, after slight alterations were made in the geometry of the fillet regions. With the fringe pattern of Fig. 6 serving as a guide, a preliminary attempt was made by hand filing the original disk lug template in the two central fillet regions. The original model was then rerouted following the modified template, and isochromatic patterns of the rerouted model were photographed. After further hand filing, the process was repeated.

The isochromatics obtained from these two modified geometries of the disk lug are shown in Fig. 16. Both show a definite reduction in the fringe order in the fillet compared with the pattern shown in Fig. 6. All these patterns are for the same load. The reduction in fringe order indicates a reduction in the s.c.f. However, because the modifications were made on an old model, because they were made by hand, and because only the two central fillets were modified, no quantitative determination of the s.c.f. was deemed advisable from this model.

A new template of the disk model was made with the 0.1875 in. (4.76-mm) fillet radius (0.055 in. (1.40 mm) in the engine) replaced with a 0.819 in. (20.8-mm) radius (0.240 in. (6.10 mm) in the engine) having the same tangent point with the bearing surface, and with the center of the 0.290 in. (7.37-mm) radius (0.085 in. (2.16 mm) in the engine) shifted to be tangent with the new radius. The original and modified dimensions are shown in Fig. 17. The modification was made on all four fillets of the disk model.

The isochromatic pattern for the same load as those of Figs. 6 and 16 is shown in Fig. 18. The maximum fringe in the fillet seems to fall somewhere between the fringes of the two modifications in Fig. 16. The s.c.f. from the pattern in Fig. 18, determined as described previously, is compared with the s.c.f.'s shown on page 12, in Table 4

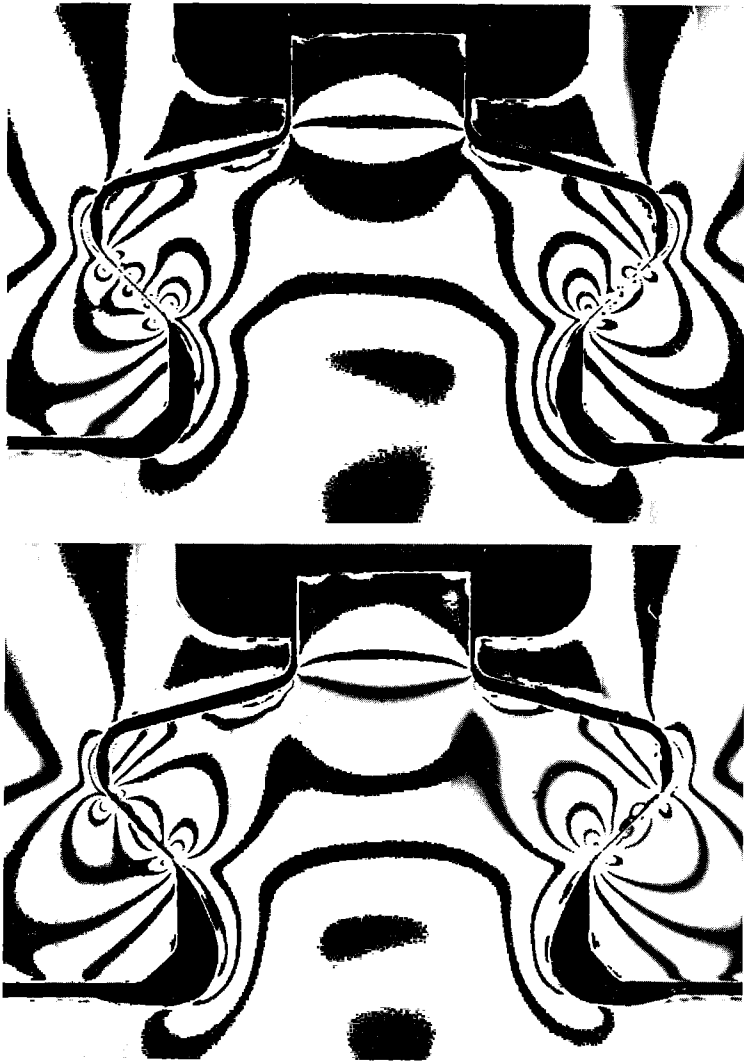


Fig. 16 — Dark field isochromatic pattern of two modifications of the disk lug with fillet radius increased by different amounts (hand filed)

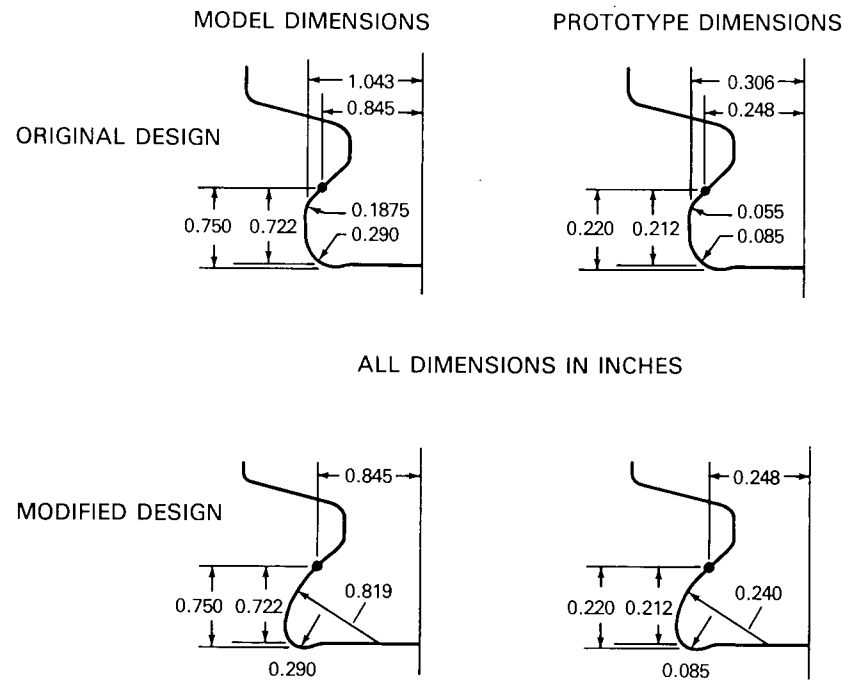


Fig. 17 — Geometric modification proposed to reduce stresses in disk fillet. The modified and original designs both have the same point of tangency between the fillet radius and the bearing surface. (1 inch = 25.4 mm).



Fig. 18 — Dark field isochromatic pattern of disk lug with modified fillet radius 4.36 times original design radius

The analysis shows a 27% reduction in the fillet stress of the disk. The stresses along the fillet boundary, comparable to those given in Fig. 11, are shown in Fig. 19.

The blade geometry could not be modified in the same way as that of the disk lug, since an increase in the blade fillet radius of the same amount might undercut the blade platform.

These results indicate that an appreciable decrease of the fillet stress can be made by slight modification of the geometry. Accordingly, an "ideal" or "optimized" fillet can be imagined. The ideal fillet can be defined as that fillet which would have the lowest stress for the given loading condition without changes in geometry that would affect other design requirements.

Experience indicates that the ideal fillet is approached as the maximum isochromatic fringe in the fillet area is reduced and remains parallel to the boundary over a greater distance along the boundary. This can be thought of as reducing the peak stresses by spreading the high stress over a larger area. Notice that the isochromatic pattern at the

Table 4 — S.C.F. for Original and Modified Disk Fillet

Disk Geometry	Disk Fillet	Blade Fillet
Original	5.2	4.8
Modified	3.8	4.8

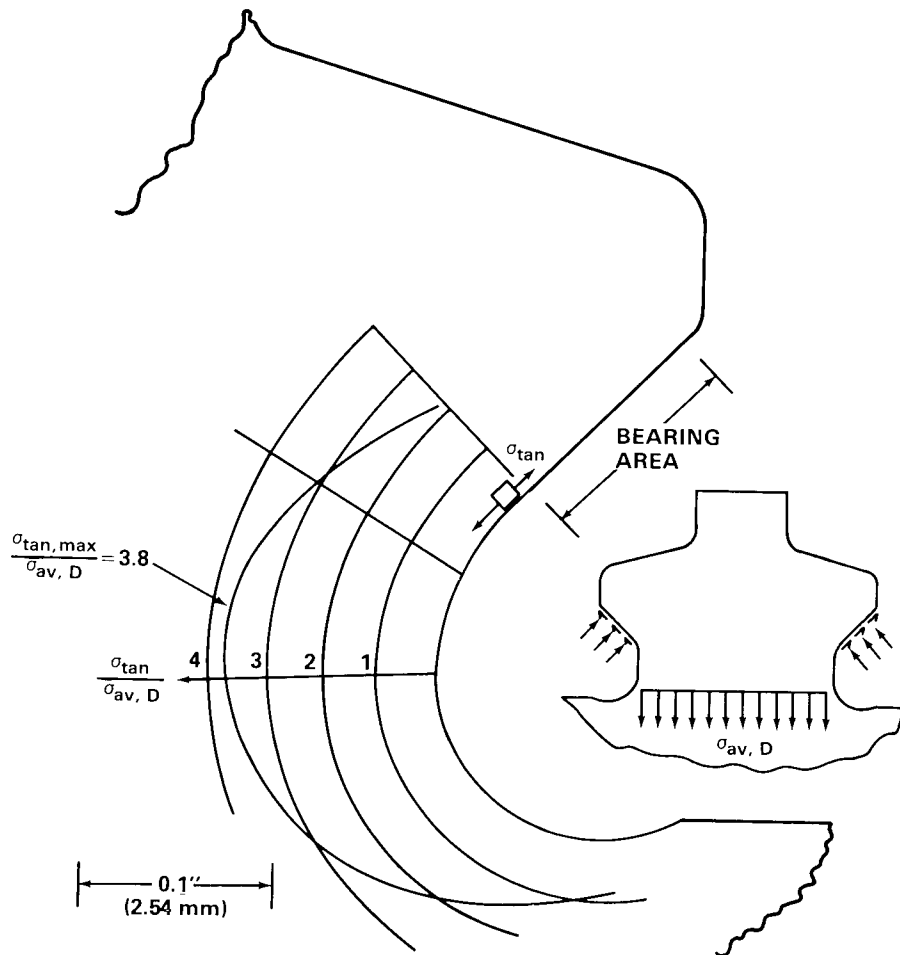


Fig. 19 — Tangential boundary stress in fillet of disk with improved design geometry

pattern of Fig. 18. However, the contour of the fillet region in the bottom of Fig. 16 has a continuing change in radius, thus making machining by most techniques difficult or costly for the prototype structure. For this reason it is preferable to vary a single radius systematically, so that each new geometry can be simply machined.

In any case, it should not be assumed that the s.c.f. could be reduced to unity. Heywood's analysis (described in the Appendix) suggests that the reduction of the s.c.f. in the disk fillet could be no more than 43% (from 5.2 to 3.0). The reduction is limited because the fillet stress is due to a bending action rather than to a direct tensile load on the disk lug.

STRESSES ON THE BEARING SURFACE ADJACENT TO THE FILLET

As mentioned above, the position, direction, distribution, and even the magnitude of the bearing load vary greatly from tooth to tooth and over the bearing surface of each tooth. The loads used in the theoretical solution of the problem, and even those obtained in the experimental work, were representative idealizations of these varied loads. Some indication has been given above concerning how much these varied loads influence the fillet stresses.

A bearing load often has a maximum at the very edge of the contact zone. A maximum of this sort would produce a high compressive normal stress just adjacent to the fillet. In addition to the compressive stress in the contact zone, bearing loads produce a tensile stress tangential to the surface just beyond the contact area, apart from tensile stress produced by bending of the tooth. The tangential tensile stresses in the fillet analyzed and reported above continue into the bearing area, and they are superimposed on whatever compressive stresses and tensile stresses are produced by the local bearing load. This tangential tensile stress component decreases through the bearing area in a more or less linear manner.

It has been speculated that the primary mechanism of failure of the disk lugs is a fretting fatigue at or near the inner edge of the bearing area. Fretting fatigue results from high compressive bearing forces normal to the boundary combined with cyclic tensile stresses parallel to the boundary. The photoelastic study reported here shows that the modified design would reduce the tangential tensile stress in the region of failures by about 50% and presumably would reduce the chances of fretting failures.

SUMMARY

The stress concentration factor in the disk fillet was found to be 5.2. Distributions of stress along the fillet boundary and along interior lines in the disk are reported in Figs. 11, 13, and 15.

The stress concentration factor in the blade fillet was found to be 4.8. Distributions of stress along the blade fillet boundary and along one interior line of the blade are reported in Figs. 12 and 14.

A preliminary modification of the disk fillet geometry indicates that a 27% reduction in the stress concentration factor is possible with the existing disks by removing material in the relief area between the disk lug and the blade.

Appendix A

STRESS CONCENTRATION FACTORS BY HEYWOOD'S METHOD

A great amount of analysis has been done by Heywood [5,6] to determine stress concentration factors (s.c.f.'s) in the fillets of teeth of machine parts. A formula developed by Heywood and modified by Kelley and Pedersen [7] is widely used for application to gear teeth, teeth of the dovetail slots of turbines, and of turbine blades, and to screw-thread teeth. The formula was recently republished [8]. The formula is based on the geometry of the two-dimensional cross section of the tooth, Fig. A-1, and on the magnitude, position, and direction of the load, which data must be specified.

There are at least two versions of Heywood's formula (5,6). The versions are similar. The version used here to analyze the s.c.f. in the fillet of the disk and blade is a modification of the one in references (6) and (7).

The formula as given in Ref. 7 is

$$\sigma = K_t \frac{P}{t} \left\{ \frac{1.5a}{e^2} + \frac{0.45}{\sqrt{(be)}} + \frac{\sin \beta}{2e} \right\},$$

where

σ is the local stress in the fillet due to a load P on the tooth

K_t is $(1 + 0.26 (e/R)^{0.7})$

R is the fillet radius

b is the distance from the load to the point of maximum stress in the fillet point M in Fig. A-1. (This point is taken as 30° from the point of tangency, point T .)

e is the distance from the tooth centerline to the point of maximum stress in the fillet

a is the distance from the load line to the point on the tooth centerline from which e is measured

t is the thickness

β is the angle defining the direction of load with respect to the tangent line through the fillet at the point of maximum stress (see Fig. A1).

This formula was modified by dividing both sides by the average stress in the minimum section of the disk lug, P'/tw . This normalized the stress and gave the desired s.c.f. The formula was further modified by replacing the load P on the tooth with an expression containing the radial load on the blade, P' . The modified formula is

$$\frac{\sigma}{P'/tw} = \left[1 + 0.26 \left(\frac{e}{R} \right)^{0.7} \right] \left[1.5 \left(\frac{a}{e} \right) + 0.45 \left(\frac{e}{b} \right)^{0.5} + \frac{\sin \beta}{2} \right] \left[\frac{w}{e} \right] \left[\frac{1}{2 \cos (45^\circ - \gamma)} \right],$$

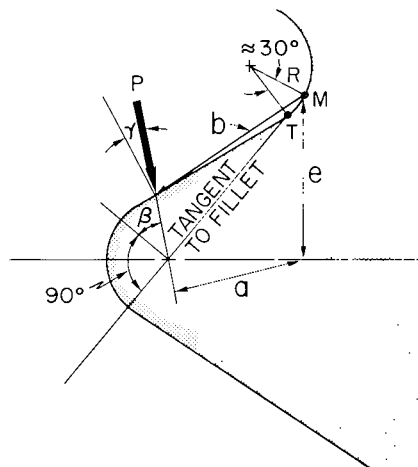


Fig. A-1 — Notation used in heywood formulation for stress concentration factors in fillets

where w is the width of the disk lug and γ is the angle between the direction of load and the normal to the loaded surface. When the contact is friction free, $\gamma = 0$; for a coefficient of friction of 0.16, $\gamma = \arctan(0.16) = 9^\circ$.

Heywood [6] suggests combining his formula with Neuber's analysis to account for the stresses due to loads which pass through the net section but are taken up by teeth farther from the load. Since here there is only one pair of teeth, this was not done. However, the concept of s.c.f. due to the load on the net section as opposed to a s.c.f. due to the loading on the tooth, indicates a complexity of the loading that should be recognized.

Values of R and w were taken from the manufacturing drawings. Values of e , b , a , and β were determined from oversize drawings (27.3X actual or 8X model), with the load applied at the center of bearing surface of the tooth. The values used are shown in Table A-1.

Table A-2 shows the normalized stresses obtained from the formula compared to those obtained from photoelastic analysis.

Although the actual photoelastic analysis is more reliable than the general formula of Heywood, a great deal can be learned by considering the various components of Heywood's analysis.

Table A-1 — Values Used in Heywood's Formula

	Disk		Blade	
R	0.055		0.055	
e	0.122		0.156	
b	0.082		0.088	
w	0.505		0.505	
	No Friction	Friction	No Friction	Friction
a	0.022	0.038	0.025	0.047
β	30°	39°	30°	39°
γ	0°	9°	0°	9°

Table A-2 — Comparison of Stress Concentration Factors

	Disk		Blade	
	No Friction	Friction	No Friction	Friction
Formula	4.54	4.95	3.85	4.22
Photoelasticity		5.2		4.8

To apply Heywood's formula it was necessary to specify the position, magnitude, and direction of a point load on the tooth, equivalent to the actual position, magnitude, and direction of the actual distributed load. For Heywood's analysis, the *position* of the load was chosen at the center of the bearing area. Two *directions* were considered: one assuming no friction required the load to act normal to the bearing surface; the other assumed a coefficient of friction of 0.16 and required the load to act at 9° to the bearing surface. By specifying the direction, and assuming equal loads on both teeth of the blade (symmetry), *magnitude* of the load is determined from equilibrium. In summary, the assumptions that the load acts at the center of the tooth, is symmetric on both sides of the blade, and has a certain coefficient of friction, determine all the terms in Heywood's formula.

With these restrictions in mind, it is possible to consider the various physical phenomena as depicted by Heywood's formula. Thus, increasing friction increases γ and β and increases the s.c.f., but the increase is less than if only a change in γ is considered. Changing the position of load increases the s.c.f. on either the blade or disk while simultaneously decreasing it on the other. This is quantified by changing a , and also changing b . The influence of b is less, but tends to offset changes in a slightly. Increasing the fillet radius decreases the K_t factor. The width of the neck of the disk, w , is reduced at the expense of increasing the fillet radius, and so the average stress is increased. However, the overall effect, up to a certain point, is a reduction in the s.c.f. Finally, it is seen that the s.c.f. is unchanged by changing the magnitude of load so long as the loading is assumed symmetric.

These considerations of Heywood's analysis are helpful in two ways. First, they indicate the influence of variation of the position and direction of the load on the stresses in the fillets. Second, they provide guidance for the geometric changes that can be made to reduce the stresses in the fillets.

REFERENCES

1. M. E. Fourney and K. V. Mate, "Further Applications of Holography to Photoelasticity," *Exper. Mech.* **10** (No. 5), 177-186 (May 1970).
2. R. J. Sanford, "A General Theory of Polarization Holography and Its Application to Photoelastic Analysis," *Engineering Applications of Holography*, SPIE, Redondo Beach, Calif., 1972, pp. 331-343.
3. R. J. Sanford and A. J. Durelli, "Interpretation of Fringes in Stress-Holo-Interferometry," *Exper. Mech.* **11** (No. 4), 161-166 (Apr. 1971).
4. R. J. Sanford, "Fringe Patterns in Photoelastic Holography," *Progress in Exper. Mech.*, Catholic University of America, 1975, pp. 167-190.
5. R. B. Heywood, *Designing by Photoelasticity*, Chapman and Hall, Ltd., 1952, p. 210.
6. R. B. Heywood, *Designing Against Fatigue of Metals*, Reinhold, 1962, p. 262.
7. B. W. Kelley and R. Pedersen, "The Beam Strength of Modern Gear-Tooth Design," *SAE Trans.*, **66**, 137-157 (1958).
8. R. J. Roark and C. W. Young, *Formulas for Stress and Strain*, McGraw-Hill, 5th ed., 1975, p. 157 (p. 132 in 4th ed., 1965).

